Applied Surface Science 256 (2010) 3438–3442

Contents lists available at ScienceDirect

Applied Surface Science

journal homepage: www.elsevier.com/locate/apsusc

The role of nitrogen in the preferential chromium segregation on the ferritic stainless steel (1 1 1) surface

J. Yuhara [a,*], T. Matsui [a,b]

[a] School of Engineering, Nagoya University, Furo-cho, Chikusa-ku, Nagoya 464-8603, Japan
[b] Ecotopia Science Institute, Nagoya University, Furo-cho, Chikusa-ku, Nagoya 464-8603, Japan

ARTICLE INFO

Article history:
Received 14 July 2009
Received in revised form 14 September 2009
Accepted 15 December 2009
Available online 28 December 2009

Keywords:
Surface segregation
Steel
Nitrides
Carbides
Scanning tunneling microscopy

ABSTRACT

The temperature dependence on the segregation behavior of the ferritic stainless steel single crystal (1 1 1) surface morphology has been examined by scanning tunneling microscopy (STM), Auger electron spectroscopy (AES), and low energy electron diffraction (LEED). AES clearly showed the surface segregations of chromium and nitrogen upon annealing. Nanoscale triangular chromium nitride clusters were formed around 650 °C and were regularly aligned in a hexagonal configuration. In contrast, for the ferritic stainless steel (1 1 1) surface with low-nitrogen content, chromium and carbon were found to segregate on the surface upon annealing and Auger spectra of carbon displayed the characteristic carbide peak. For the low-nitrogen surface, LEED identified a facetted surface with (2×2) superstructure at 650 °C. High-resolution STM identified a chromium carbide film with segregated carbon atoms randomly located on the surface. The facetted (2×2) superstructure changed into a (3×3) superstructure with no faceting upon annealing at 750 °C. Also, segregated sulfur seems to contribute to the reconstruction or interfacial relaxation between the ferritic stainless steel (1 1 1) substrate and chromium carbide film.

1. Introduction

Ferritic stainless steels have gained acceptance in automotive exhaust systems, containers, fast reactors for power generation, and other functional applications. These steels can be fabricated at low cost and exhibit good corrosion resistance, low thermal expansion and high thermal conductivity compared with austenitic stainless steel [1]. Since corrosion resistance is closely related to the segregation properties of alloys and impurities, many researchers have studied the temperature dependence of surface concentrations and microstructures [2,3].

The segregated components on stainless steel single crystal surfaces have been studied so far using X-ray photoelectron spectroscopy, Auger electron spectroscopy (AES), and scanning electron microscopy [4–6]. Scanning tunneling microscopy (STM) is a powerful and well-established technique for probing morphology and surface structures down to atomic resolution [7]. However, no direct observations by STM have been reported on the stainless steel surface, except Lin et al. for the $Fe_{0.8}Cr_{0.2}$ (1 0 0) surface [8]. Therefore, little is known concerning the relationship between nanoscale morphology and segregated impurities.

In the present work, the relationship between nanoscale morphology and segregated impurities of single crystals of ferritic stainless steel is investigated by means of STM, AES, and LEED. Among the low index surface, we used (1 1 1) oriented ferritic stainless steel single crystals. Ferritic stainless steel single crystals with different low-nitrogen contents were used to investigate the influence of nitrogen on the chromium surface segregation.

2. Experimental

The experiments were performed in an ultrahigh vacuum (UHV) chamber operating at a base pressure less than 5×10^{-10} mbar in the sample preparation chamber and 4×10^{-11} mbar in the analysis chamber. The system is equipped with a rear view LEED system operating with a LaB_6 filament. Four-grid optics allows retarding field Auger analysis. STM measurements employed a commercially available UHV STM-1 system (Omicron), designed for room temperature measurement. All apparatus are on an air damper with an active vibration isolation system (Kurashiki). All STM images shown here were acquired with W tips, electrochemically etched in KOH solution. Sample heating was accomplished through electron bombardment from a thoriated iridium filament placed behind the sample plate at an emission current of 20–30 mA and a voltage of 500–700 V. The temperatures were monitored by a radiation thermometer and

* Corresponding author.
E-mail address: j-yuhara@nucl.nagoya-u.ac.jp (J. Yuhara).

0169-4332/$ – see front matter © 2009 Elsevier B.V. All rights reserved.
doi:10.1016/j.apsusc.2009.12.048

type K thermocouple mounted on the tantalum clip of the sample holder.

The specimens used were a single crystal (1 1 1) surface of the AISI 430 ferritic stainless steel (MaTecK GmbH, Germany). The orientation accuracy of the single crystal was estimated to be $<0.1^\circ$ from Laue picture. The bulk composition ratio in weight percent (wt.%) is as follows: Cr $\sim$ 16, C $<$ 0.12, Si $<$ 0.75, Mn $<$ 1.0, P $<$ 0.04, S $<$ 0.03, N $<$ 0.03, Ni $<$ 0.6, balance Fe. The sample was sputtered by 2 keV Ar^+ ions at room temperature, followed by annealing for 15 min at the temperature of interest and all measurements were subsequently made at room temperature. STM images were acquired in constant current mode with positive sample bias voltage to estimate the surface morphology and the size of nanoclusters. The elemental concentrations in the surface were studied by AES. We have semi-quantitatively determined the atomic concentrations using sensitivity factors in the literature [9] from the Fe *LMM* (702 eV), Cr *LMM* (527 eV), C *KLL* (272 eV), S *LMM* (151 eV), O *KLL* (510 eV), N *KLL* (380 eV), and P *LMM* (120 eV) peak-to-peak heights. It is noted that the mean free path of electrons in the energy range from 120 to 700 eV is 0.5–1.5 nm. The surface structure was studied by LEED at incident energies between 20 and 180 eV. To prepare the low-nitrogen content ferritic stainless steel sample, the specimen was repeatedly annealed at high temperature (950 °C) under UHV conditions to enhance the nitrogen migration to the surface and desorption from the ferritic stainless steel. The bulk nitrogen composition is estimated from AES to be $<$0.003 from annealing experiments.

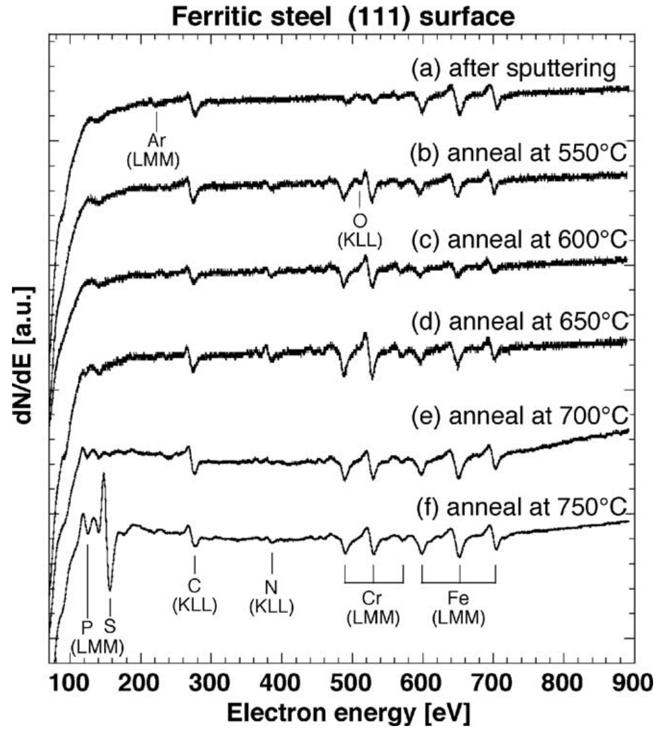

Fig. 2. AES spectra of the ferritic stainless steel (1 1 1) surface after sputtering (a) and after annealing at 550 °C (b), 600 °C (c), 650 °C (d), 700 °C (e), and 750 °C (f).

3. Results

In Section 3.1, we present results from the ferritic stainless steel (1 1 1) surface. In Section 3.2, we present the results from the low-nitrogen content ferritic stainless steel (1 1 1) surface.

3.1. Ferritic stainless steel (1 1 1) surface

Fig. 1 shows STM images of the ferritic stainless steel (1 1 1) surface after annealing at 550 °C (a), 650 °C (b), and 750 °C (c). Only a disordered surface is seen at the annealing temperature of 550 °C. The surface roughness is found to be about 0.1 nm. The inset of Fig. 1(a) shows a close-up view of clusters with a diameter of 1 nm imaged by high-resolution STM. Upon annealing at 650 °C, nanoscale triangular clusters of similar size are observed. These nanoclusters exhibit a preferential orientation with respect to the (1 1 1) surface. The side lengths of the nanoclusters are estimated to be about 2–3 nm from STM images. Their heights are also estimated to be about 0.2–0.3 nm. The nanoclusters are all aligned, forming a hexagonal configuration. Upon annealing above 750 °C, most of these nanoclusters become smaller and are positioned randomly, keeping the preferential orientation. At any stage of the annealing, steps are not observed in the STM images over a scanning area of several millimeters, although the surface is oriented $<0.1^\circ$ away from the (1 1 1) face.

Fig. 2 shows AES spectra of the ferritic stainless steel (1 1 1) surface after sputtering and after annealing at temperatures ranging from 550 to 750 °C. Enrichments of chromium and nitrogen are seen after annealing, reaching a maximum concentration at the temperature of 650 °C. The surface atomic concentration ratios of Cr:N after sputtering and after annealing at 650 °C are estimated to be 10%:0%, and 33%:12%, respectively. The segregation and dissolution behaviors of chromium agree well with those of nitrogen. The phosphorous and sulfur signals are seen above 700 °C. The oxygen signals are seen after sputtering and after annealing at 550 °C. The C signals are observed at all stages of

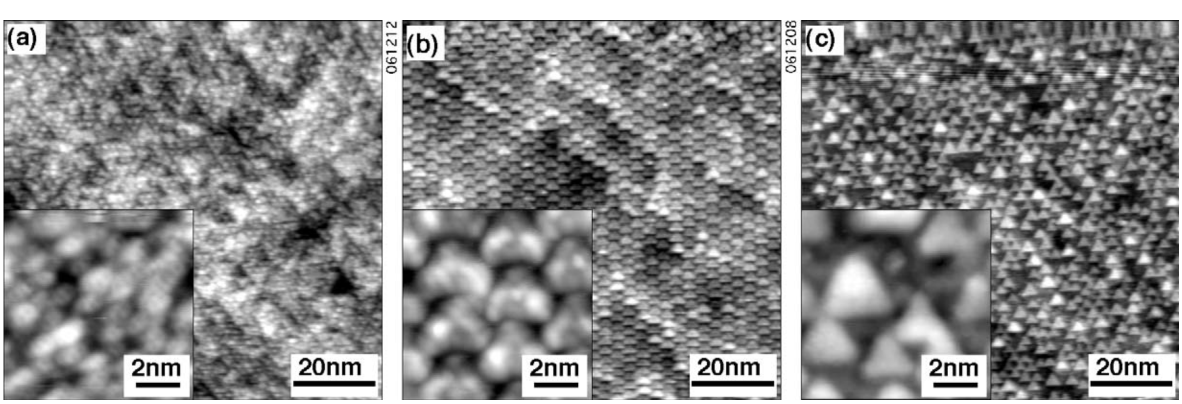

Fig. 1. Large-scale STM images (100 nm × 100 nm) of ferritic stainless steel (1 1 1) surface after annealing at the temperatures of 550 °C (a), 650 °C (b), and 750 °C (c). The insets show high-resolution STM images (10 nm × 10 nm) at the same temperatures.

the sample treatment. No carbide peaks are observed in any AES spectra. The LEED patterns only showed faint 1×1 spots after annealing.

3.2. Low-nitrogen content ferritic stainless steel (1 1 1) surface

A ferritic stainless steel with low-nitrogen content was prepared by repeated high temperature annealing at 950 °C in order to remove the nitrogen from the bulk. Fig. 3 shows STM images of this low-nitrogen ferritic stainless steel (1 1 1) surface after annealing in the temperature range from 550 to 750 °C. Upon annealing at 550 °C, the surface is atomically well-ordered, but a number of local maxima of round shape are observed. These maxima are located at the positions of minima on the atomically ordered surface. The number of local maxima increases at 650 °C and decrease at 750 °C, as shown in Fig. 3(b) and (c). The atomic steps are clearly observed, and the triangular nanoclusters as is seen in Fig. 1 were not observed in this surface. N_2 gas at a partial pressure of 2×10^{-8} mbar was exposed to this surface during annealing to examine the formation of CrN triangular nanoclusters. However, no clusters were formed.

Fig. 4 shows the AES spectra of the low-nitrogen ferritic stainless steel (1 1 1) surface after sputtering and after annealing. The nitrogen peaks are shown to be almost background level; meaning nitrogen was almost fully removed from the bulk. The chromium and carbon peaks increase after annealing. The phosphorous and sulfur signals are seen only above 650 °C. Both chromium and carbon concentrations reach a maximum at 650 °C. These results indicate that chromium co-segregates with carbon.

Fig. 5 shows typical LEED patterns of the low-nitrogen ferritic stainless steel (1 1 1) surface after annealing. After annealing at 550 °C, triangular diffuse spots with high background intensity are observed, as shown in Fig. 5(a). After annealing at 650 °C, a splitting of the (2×2) pattern is seen, producing sharp extra spots in the form of triangular rosettes around the original (1×1) pattern, as shown in Fig. 5(b). As discussed later, these extra sharp spots are attributed to be facet spots. Further annealing at 750 °C results in the formation of a (3×3) structure, as shown in Fig. 5(c). No splitting of the diffraction spots is observed. Fig. 6 shows typical wide-scale STM image of the low-nitrogen ferritic stainless steel (1 1 1) surface after annealing at 650 °C. The faceting overlayer films are clearly observed.

4. Discussion

Concerning the chromium segregation at the ferritic stainless steel (1 1 1) surface under UHV conditions, i.e. an oxygen free atmosphere, the AES spectra in Fig. 2 clearly showed that chromium segregates on the surface much more than the

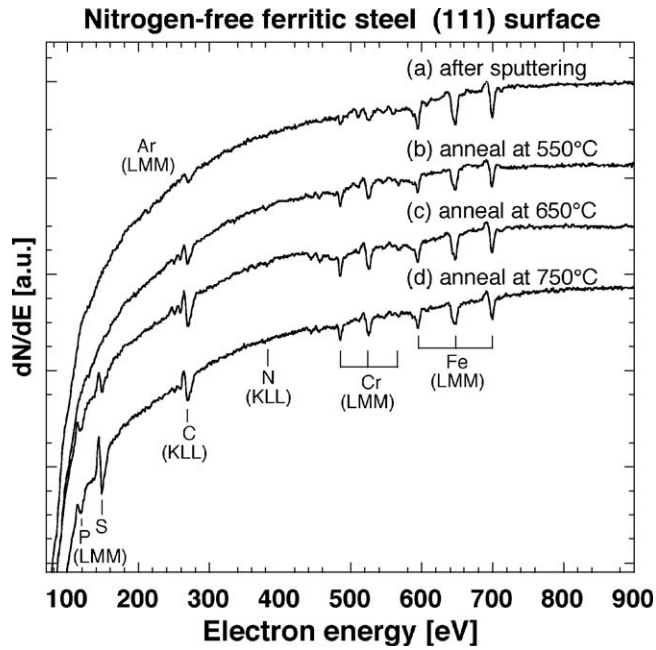

Fig. 4. AES spectra of low-nitrogen ferritic stainless steel (1 1 1) surface after sputtering (a) and after annealing at 550 °C (b), 650 °C (c), and 750 °C (d).

theoretical Cr surface concentration calculated by using density functional theory in combination with the generalized gradient approximation [10]. We also find by AES in Fig. 2 that nitrogen also segregates on the surface, which plays an important role in stabilizing the segregated chromium at the surface. This conclusion is confirmed by lower intensity peaks of Cr and N in AES spectra at the low-nitrogen content surface, as shown in Fig. 4. We propose that the strong chemical interaction between chromium and nitrogen causes strong chromium segregation, resulting in a chromium nitride formation. These results agree well with other, similar studies on single and polycrystalline surfaces of austenitic stainless steels and iron chromium alloys [4,8,11,13].

From the STM images, we showed that chromium nitride forms triangular nanoclusters fully covering the surface. The nanoclusters are well-ordered and have similar size and shape after annealing at 650 °C, resulting in the regularly aligned hexagonal configuration with respect to the (1 1 1) surface. Based on the preferential orientation of the threefold triangular nanoclusters, we conclude that chromium and nitrogen form cubic structure, CrN, on the surface. The CrN formation is consistent with previous studies [4,8,11,12]. Their side lengths and heights are estimated to be about 2–3 nm and 0.2–0.3 nm, respectively. Their ratio of side

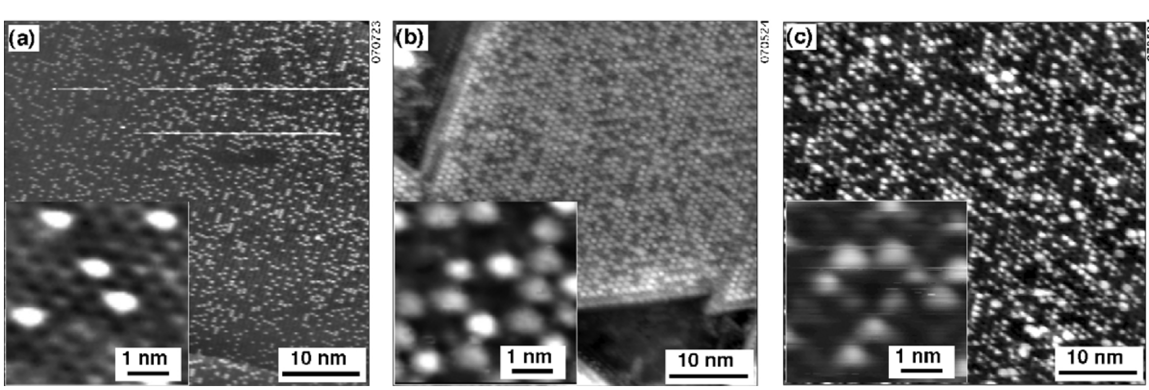

Fig. 3. Large-scale STM images (50 nm × 50 nm) of low-nitrogen ferritic stainless steel (1 1 1) surface after annealing at 550 °C (a), 650 °C (b), and 750 °C (c). The insets show high-resolution STM images (5 nm × 5 nm) at the same temperatures.

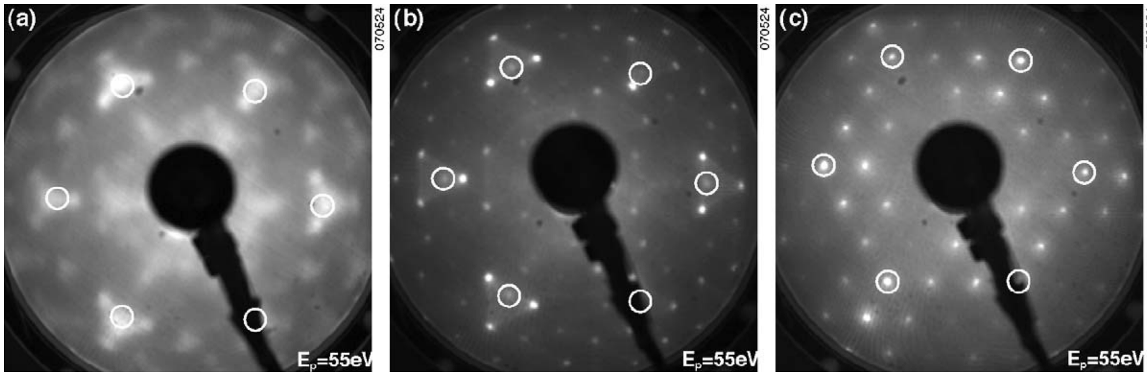

Fig. 5. LEED patterns at 55 eV incident electron energy of low-nitrogen ferritic stainless steel (1 1 1) surface after annealing at 550 °C (a), 650 °C (b), and 750 °C (c). The first-order ferritic stainless steel (1 1 1) substrate spots are marked by open circles.

length to height is thus approximately 10:1. Since the atomic spacing of the CrN (1 1 1) surface is 0.18 nm, we propose that the observed nanoclusters are one or two atomic layers in height. Since the three-dimensional nanoclusters cover the entire surface

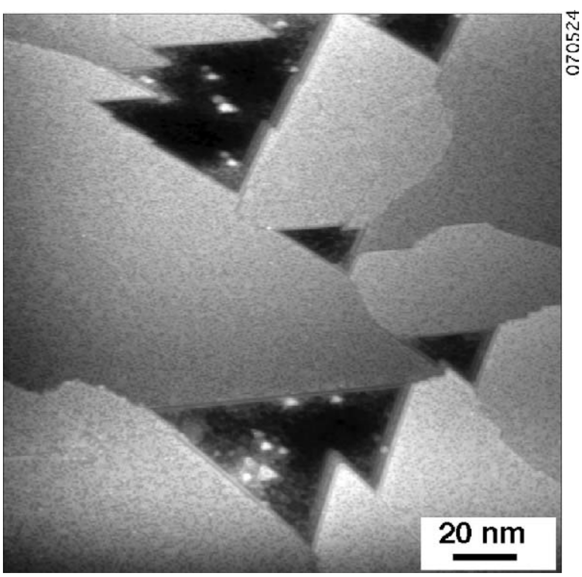

Fig. 6. Wide-scale STM image (200 nm × 200 nm) of low-nitrogen ferritic stainless steel (1 1 1) surface after annealing at 650 °C.

including step edges, no steps are clearly observed on the surface. Upon further annealing at higher temperature at 750 °C, however, the CrN nanoclusters begin shrink, and the resulting smaller triangular clusters remain randomly positioned on the surface. Since the segregation of sulfur and phosphorus was observed only above 650 °C, we conclude these elements do not directly influence the chromium segregation. The role of carbon is also not clear in the present study.

The low-nitrogen ferritic stainless steel (1 1 1) surface after annealing at 550 °C showed no triangular nanoclusters in the STM images, as shown in Fig. 3. STM images identified the atomic scale ordering with local maxima at the position of minima on the atomically ordered surface. The LEED patterns showed unique triangular rosettes around the original (1 × 1) pattern, as shown in Fig. 5(b). AES showed that the surface concentrations of chromium and carbon increased after annealing at 550 °C and Auger carbon spectra display the characteristic carbide peaks in the energy range from 250 to 270 eV [9]. Sulfur and phosphorous intensities, on the other hand, started to increase after annealing above 650 °C. We therefore conclude that a chromium carbide film is formed at the surface, inducing surface faceting and resulting in the splitting of the (2 × 2) LEED pattern.

The schematic diagrams of LEED patterns are shown in Fig. 7 for thin films with slightly contracted unit cell compared to the substrate and for tilted thin films with slightly contracted unit cell with single and multi domains. The splitting (2 × 2) LEED pattern that has triangular rosettes around the original (1 × 1) pattern in Fig. 7(c) is shown to be very similar to the observed LEED pattern in

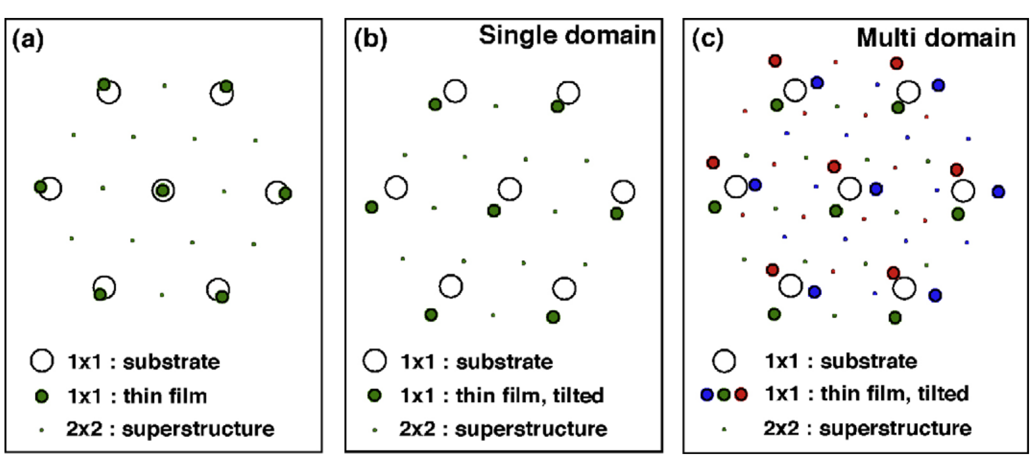

Fig. 7. Schematic diagrams of LEED patterns for thin films with slightly contracted unit cell compared to the substrate (a) and for tilted thin films with slightly contracted unit cell with single (b) and multi (c) domains.

Fig. 5(b). As deduced from the distance between these spots, the contraction of the unit cell in the chromium carbide thin film is estimated to be 7%. Since the lattice constant for the ferritic stainless steel is 0.286 nm, the lattice constant for the chromium carbide thin film is calculated to be 0.265 nm. From a variety of chromium carbide compounds [14], only a $Cr_{23}C_6$, whose lattice constant is 1.06 nm, matches a coincidence structure. Since the substrate is (1 1 1) surface, 6 interatomic spacing of the $Cr_{23}C_6$ (1 1 1) thin film fits onto 4 interatomic spacing on the steel substrate. The orientation angle of the thin film tilted from the (1 1 1) steel surface is estimated to be $\sim 7^{\circ}$ from the LEED pattern in Fig. 5(b). Direct observation by wide-scale STM also identified the faceting films, as shown in Fig. 6. The large lattice mismatch between the substrate and the thin film may be related to the misorientation of the film growth.

The concentration of local maxima seen in the STM images in Fig. 3 initially increased with annealing temperature, then slightly decreased upon annealing at 750 °C. The surface concentrations of chromium and carbon by AES also slightly decreased at 750 °C, while the sulfur concentration increased. The LEED patterns changed from the splitting of (2×2) spots into sharp (3×3) spots after annealing at 750 °C. Therefore, the local maxima are attributed to segregated C impurities and not directly related to the surface structures of (2×2) and (3×3). These results are in good accordance with previous study on the local structure of segregated species on Fe(1 0 0) surface [15]. Moreover, since the sulfur concentration increased and the LEED pattern splitting disappeared after annealing at 750 °C, the segregated sulfur atoms may contribute the reconstruction or interfacial relaxation between the ferritic stainless steel (1 1 1) substrate and the chromium carbide film, resulting in the structural transformation from (2×2) into (3×3) structures.

For the corrosion property, nitrogen in the bulk is significantly important in the case of no oxygen atmosphere, since it is found that chromium co-segregate with nitrogen forming chromium nitride clusters at a surface or interface. Without nitrogen, the surface or interface are mainly covered by chromium carbide films. It is also found that phosphorus seems not to contribute the chromium nitride and carbide films and sulfur may contribute the interfacial relaxation between carbide films and steel substrate at high temperature.

5. Summary

The segregation of chromium and nitrogen on the (1 1 1) oriented single crystal surfaces of ferritic stainless steel was studied in the temperature range from 550 to 750 °C by means of STM, AES, and LEED. A strong chemical interaction between Cr and N caused simultaneous segregation.

At temperatures around 650 °C, chromium and nitrogen form triangular CrN nanoclusters which enhance the strong segregation of chromium and nitrogen. At higher annealing temperatures, the CrN nanoclusters become smaller and the surface concentrations of Cr and N decrease.

For the samples with low-nitrogen content, chromium and carbon segregate to the surface upon annealing, resulting in the formation of $Cr_{23}C_6$ (1 1 1) film at temperatures up to 650 °C. The lattice mismatch of the film and the substrate induces faceting. At higher temperatures, we find that segregated S seems to contribute the reconstruction or interfacial relaxation between the chromium carbide film and the stainless steel surface.

Acknowledgments

We gratefully acknowledge the technical assistance of Mr. T. Sumi and Mr. K. Kumazawa at the machine workshop at the school of engineering, Nagoya University. This work was financially sponsored by the Innovative Nuclear R&D Program of the Ministry of Education, Culture, Sports, Science and Technology (MEXT).

References

[1] J.H. Magee, in: S.D. Henry, et al. (Eds.), ASM Handbook: Friction, Lubrication, and Wear Technology, vol. 18, ASM International, Metals Park, OH, 1992.
[2] H.J. Grabke, H. Viefhaus, in: P.A. Dowden, A. Miller (Eds.), Surface Segregation and Related Phenomena, CRC Press, Boca Raton, FL, 1990.
[3] M.P. Seah, Surf. Sci. 53 (1975) 168.
[4] U. Fehrmann, H.J. Mussig, F. Storbeck, R. Thielsch, K. Uhlmann, Kristall. u. Technik. 15 (1980) 455.
[5] C. Uebing, H. Viefhaus, H.J. Grabke, Fresenius J. Anal. Chem. 346 (1993) 275.
[6] M. Lampimaki, K. Lahtonen, P. Jussila, M. Hirsimaki, M. Valden, J. Electron Spectrosc. Relat. Phenom. 154 (2007) 69.
[7] G. Binnig, H. Rohrer, Surf. Sci. 136 (1983) 236.
[8] J.S. Lin, H. Cabibil, B. Ekstrom, J.A. Kelber, Surf. Sci. 371 (1997) 337.
[9] L.E. Davis, N.C. MacDonald, P.W. Palmberg, G.E. Riach, R.E. Weber, Handbook of Auger Electron Spectroscopy, 2nd ed., Physical Electronics Industries, Eden Prairie, 1976.
[10] M. Ropo, K. Kokko, M.P.J. Punkkinen, S. Hogmark, J. Kollár, B. Johansson, L. Vitos, Phys. Rev. B 76 (2007) 220401(R).
[11] C. Uebing, V. Scheuch, M. Kiskinova, H.P. Bonzel, Surf. Sci. 321 (1994) 89.
[12] R. Louahdi, V. Hayes, R. Marchand, G. Saindrenan, J. Phys. IV: France 123 (2005) 105.
[13] C. Uebing, H. Viefhaus, H.J. Grabke, Appl. Surf. Sci. 32 (1988) 363.
[14] J.T.H. Pearce, D.W.L. Elwell, J. Mater. Sci. Lett. 5 (1986) 1063.
[15] J. Fujii, M. Galaktionov, L. Giovanelli, G. Panaccione, F. Bondino, I. Vobornik, G. Rssi, Thin Solid Films 428 (2003) 30.